REPORT DOCUMENTATION PAGE

Form Approved
OMB No. 0704-0188

1. REPORT DATE (DD-MM-YYYY)	2. REPORT DATE	3. DATES COVERED (From - To)
15/03/2003	15/03/2003	10/01/2001 - 31/12/2002

4. TITLE AND SUBTITLE
~~Mine Detection Modeling and Simulation in a Random Environment~~

5a. CONTRACT NUMBER

5b. GRANT NUMBER
N00014-01-1-0189

5c. PROGRAM ELEMENT NUMBER
N00014-01-1-0189

6. AUTHOR(S)
Roger Ghanem/
Dubar Kamar (Master thesis).

5d. PROJECT NUMBER

5e. TASK NUMBER

5f. WORK UNIT NUMBER

7. PERFORMING ORGANIZATION NAME(S) AND ADDRESS(ES)
Johns Hopkins University

8. PERFORMING ORGANIZATION REPORT NUMBER
N/A

9. SPONSORING/MONITORING AGENCY NAME(S) AND ADDRESS(ES)
OFFICE OF NAVAL RESEARCH
BALLSTON CENTRE TOWER ONE
800 N. QUINCY ST.
ARLINGTON VA 22217-5660

10. SPONSOR/MONITOR'S ACRONYM(S)
N/A

11. SPONSORING/MONITORING AGENCY REPORT NUMBER
N/A

12. DISTRIBUTION AVAILABILITY STATEMENT
Unlimited

13. SUPPLEMENTARY NOTES

14. ABSTRACT
Sensitivity of Ocean model predictions to boundary data is investigated. The data is modeled as Random with a probabilistic structure. This is important in interpreting the results of data assimilation and the impact of associated errors on model predictions.

15. SUBJECT TERMS
Ocean models, Karhunen-Loève, Random processes, bottom topography, Data Assimilation.

16. SECURITY CLASSIFICATION OF:			17. LIMITATION OF ABSTRACT	18. NUMBER OF PAGES	19a. NAME OF RESPONSIBLE PERSON
a. REPORT	b. ABSTRACT	c. THIS PAGE			Roger Ghanem
U	U	U	UU	60.	19b. TELEPONE NUMBER (Include area code) 410 516 7647

Standard Form 298 (Rev. 8-98)
Prescribed by ANSI-Std Z39-18

Sensitivity Analysis of Limited Area Ocean Model

by

Dubar K. Kamara

A thesis submitted to Johns Hopkins University in conformity with the requirements for the degree of Master of Science

Baltimore, Maryland

August 2002

Abstract

For a data assimilation problem for a limited-area ocean model, the boundary data can either be supplied by its global model or from observations interpolated from conventional observing network. In this study, the sensitivity of the ocean model to variations in the boundary data will be investigated. Additionally, we will be looking at how predictions of wave height are affected by variations in basin depth. Two models are used to carry out the analyses; a large scale ocean circulation model and a combined wave refraction diffraction model. The large scale circulation model is used to implement the limited area ocean model and results show that the accuracy and availability of boundary data affects the model predictions.

Contents

1 Introduction 1

1.1 Background 1

1.2 Organization of this Thesis 2

2 Model Formulation 4

2.1 Ocean Circulation 4

2.1.1 Governing Equations 5

2.2 Water Waves 7

2.2.1 Governing Equations 9

3 Sensitivity Analysis 12

3.1 Karhunen-Loeve Expansion 12

3.2 Polynomial Chaos Expansion 13

4 General Circulation Model 15

4.1 Introduction 15

4.2 Shallow Water Equations 16

4.3 Boundary Conditions 20

4.4 Bounded Derivative Method 21

4.5 Incorporating Topography 21

4.6 Sensitivity Analysis 24

4.7 Results 24

5 Water Wave Model **28**

5.1 Ref/Dif 1 28

5.2 Mild slope equation 30

5.3 Energy dissipation 32

5.4 Bottom Topography 33

5.5 Results 46

6 Conclusion **57**

List of Figures

2.1 Coordinate system of equations of motion 5

2.2 Two-dimensional wave profile 8

4.1 Contour plot of the horizontal velocity component, u over the entire basin at the first time step 25

4.2 Contour plot of the horizontal velocity component, u over half the basin with one open boundary, at the first time step 26

4.3 Contour plot of the horizontal velocity component, u over three-quarters of the basin with two open boundaries at the first time step 26

4.4 Propagation of error with time 27

5.1 First Eigenmode 36

5.2 Second Eigenmode 37

5.3 Third Eigenmode 38

5.4 Fourth Eigenmode 39

5.5 Fifth Eigenmode 40

5.6 Sixth Eigenmode 41

5.7 Seventh Eigenmode 42

5.8 Eighth Eigenmode 43

5.9 Ninth Eigenmode 44

5.10 Tenth Eigenmode 45

5.11 Bottom topography for flat bottomed model 47

5.12 Plot of wave height for flat bottomed model 48

5.13 Surface plot of flat bottomed model 48

5.14 Rendering of water surface for the flat bottomed model 49

5.15 Bottom topography of first simulation 49

5.16 Plot of wave height from first simulation 50

5.17 Surface plot of first simulation 50

5.18 Rendering of water surface of the first simulation 51

5.19 Probability density 52

5.20 Mean topography 53

5.21 Mean wave Height 53

5.22 Mean surface 54

5.23 Mean surface 54

5.24 Negative variance of bottom topography 55

5.25 Variance of surface 55

5.26 Variance of wave height 56

5.27 Variance of surface 56

Chapter 1

Introduction

1.1 Background

The assimilation of random data into ocean models has not been extensively looked at. The concern of most researchers is that the models are able to reproduce the behavior shown by collected data. A data assimilation problem involves the incorporation of observed data into the problem, usually as initial conditions. The problem is then continually updated with new sets of observed data. Data assimilation also involves the preparation of observed data such that it can be used effectively in forecasting models. It is an effective tool to have when available data is limited. For a data assimilation problem for a limited-area ocean model, the boundary data can either be supplied by its global model or from observations interpolated from conventional observing network. Either way, significant uncertainty is generated at the boundary of the model representing the limited-area. In this study, the sensitivity of the ocean model to variations in the boundary data will be investigated. The random data is

generated from a coarse-grid global ocean model to be used in a fine-grid limited-area model with open boundaries. Care must be taken in how the boundary data is selected as it has been shown that errors in the initial boundary data can propagate into the interior domain significantly affecting the stability of the solution [4].

Additionally, the sensitivity of wave height predictions due to changes in bottom topography are also investigated. The Karhunen-Loeve expansion is used to generate random data to be used for the bottom topography data. The bottom is thus parameterized, as a stochastic field in terms of a few random amplitudes associated with depth. Two different ocean models were used to implement the objectives. Ref/Dif 1 developed by Kirby and Dalrymple [6] was used to implement the bottom topography. The general ocean circulation model developed by Gerald Browning at NOAA[1] was used to implement the open boundary conditions for a limited area model. The fundamental difference between these two models is that Ref/Dif 1 is a combined refraction and diffraction model that models the propagation of water waves whereas the NOAA representation models the general ocean circulation. Hence, in Ref/Dif 1 we are solving for the wave height and water depth and in the general circulation model, for the current velocity and pressure.

1.2 Organization of this Thesis

This thesis is organized into six chapters. Chapter 2 describes how a general ocean circulation model and a water wave model are developed. Chapter 3 explains the

[1]National Oceanic and Atmospheric Administration, Boulder, CO.

methods used for the sensitivity analysis in both models. A more in-depth look into the general ocean circulation model used in this thesis is given in chapter 4. Chapter 4 also describes how data can be initialized so that it can be assimilated into the model. The results of the sensitivity analysis on the limited area model are presented in Chapter 4. Chapter 5 describes Ref/Dif 1. It also includes a description of the analysis carried out and a presentation of the results. Chapter 6 is on "Conclusions".

Chapter 2

Model Formulation

2.1 Ocean Circulation

Ocean currents are driven by a combination of the sun, wind and the earth's rotation. The most obvious interaction that drives ocean currents is that between the wind and the sea surface. The sun also drives circulation by causing variations in temperature and salinity which result in a density change. The consequence is a vertical circulation pattern called the thermohaline circulation. In general, warm surface currents flow from the equator to the poles and deep water cold currents flow from the poles to the equator. The Coriolis force, which is a result of the earth's rotation, is zero at the equators increasing to its maximum at the poles. It acts at right angles to the direction of motion. Hence it has an affect on the direction of current flow. Furthermore, another factor affecting the direction of flow is land boundaries. The combining effect of the Coriolis force and the land boundaries causes the ocean circulation to be in a circular pattern. The circulation model developed by Munk in 1950 closely

matches the actual circulation pattern in the Atlantic and Pacific Oceans. The basic equations used to describe the circulation are briefly reviewed in the following section.

2.1.1 Governing Equations

In the derivation of the equations of motion, x will be positive in the eastward direction, y in the northward and z is positive in the downward direction. The velocity components u, v and w are in the x, y, and z-direction respectively. The equations

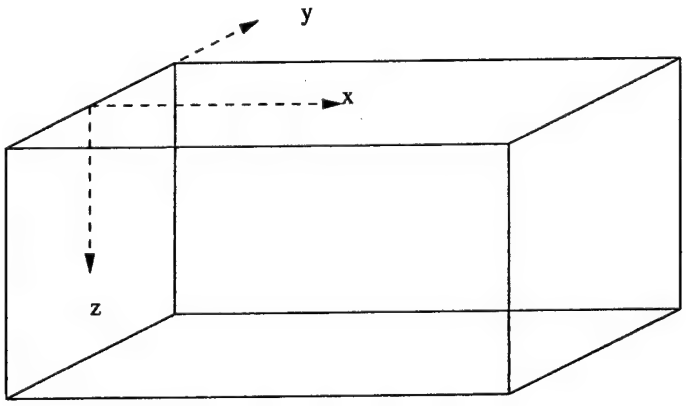

Figure 2.1: Coordinate system of equations of motion

used to describe the ocean circulation are derived from the conservation of momentum, which is Newton's second law of motion,

$$F = ma. \tag{2.1}$$

This can be re-expressed as

$$accelaration = \frac{force\ per\ unit\ volume}{density}. \tag{2.2}$$

Hence the equation of motion in the x-direction can be written as

$$\frac{du}{dt} = \frac{1}{\rho}\left(\begin{bmatrix} horizontal \\ pressure \\ gradient \\ force\ in \\ x-direction \end{bmatrix} + \begin{bmatrix} Coriolis\ force \\ resulting\ in \\ motion\ in \\ x-direction \end{bmatrix} + \begin{bmatrix} other\ forces \\ related\ to \\ motion\ in \\ x-direction \end{bmatrix}\right). \quad (2.3)$$

The observation that the Coriolis force acts perpendicular to the direction of flow is represented mathematically as

$$\frac{du}{dt} = \frac{1}{\rho}(-\frac{dp}{dx} + \rho f v + F^x), \quad (2.4)$$

where f is the Coriolis force,v is the current velocity in the y-direction, p is the pressure and ρ is the density. F^x may include wind stress, friction or tidal forcing. Similarly, the equation of motion in the y-direction is

$$\frac{dv}{dt} = \frac{1}{\rho}(-\frac{dp}{dy} - \rho f u + F^y). \quad (2.5)$$

The Coriolis force does not affect flow in the vertical direction. Hence it is not present in the vertical equation of motion. The main forces in the vertical direction are forces due to gravity and the vertical pressure gradient. Therefore the equation of motion in the z-direction can be written as

$$\frac{dw}{dt} = \frac{1}{\rho}(-\frac{dp}{dz} - \rho g + F^z). \quad (2.6)$$

As this problem involves an advective field, where a change in the field is a result of fluid motion, the time derivative is taken to be the material derivative. Hence,

$$\frac{d}{dt} = \frac{\partial}{\partial t} + u\frac{\partial}{\partial x} + v\frac{\partial}{\partial y} + w\frac{\partial}{\partial z}. \quad (2.7)$$

We will refer to the above equation as the total derivative operator.

The assumption of continuity is also used. The continuity equation in conjunction with the equations of motion provide additional constraints in the form of incompressibility.

$$\frac{\partial u}{\partial x} + \frac{\partial v}{\partial y} + \frac{\partial w}{\partial z} = 0. \tag{2.8}$$

For a global circulation model there usually is land on the lateral boundaries. Hence at the lateral boundaries the velocity normal to the boundary is set to zero. Since no flow is allowed through the sea floor at the sea bottom, the vertical velocity is set to zero. The vertical velocity is also set to zero at the sea surface. For the limited-area model the same boundary conditions will apply except at the open boundary where the flow is set to its value observed in the global model.

2.2 Water Waves

The wave height, water depth and wave length or wave period are all the characteristics needed to fully describe a wave. Figure 2.2 shows a two dimensional profile of a wave with these characteristics highlighted. Other wave characteristics such as water surface profile, the forward speed of the wave and the dynamic pressure field in the wave can be theoretically derived from the aforementioned characteristics.

The waves that are of interest to us are the surface gravity waves. With these waves, gravity is the dominant restoring force. Surface tension forces are neglected in the formulation of the wave equations. This is because surface tension forces tend to be significant only when the waves have small wavelengths, for example, of a couple centimeters and since surface gravity waves have wavelengths on the order of

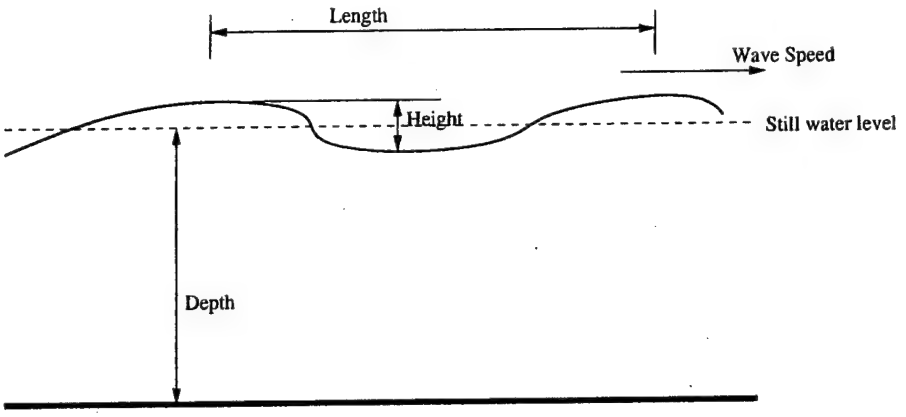

Figure 2.2: Two-dimensional wave profile

a couple meters, one can neglect surface tension forces. Some of the processes that waves undergo when they encounter an object or move into shallow water include shoaling, refraction, diffraction and dispersion. Wave refraction is the change in direction of propagation which occurs when isobaths, which are lines of constant depth, are inclined obliquely to wave fronts and can also result from wave current interactions. Diffraction is the change of wave direction due to changes in wave height along the crest. Dispersion refers to the separation of waves due to their different frequencies. That is, waves with a longer wavelength travel faster than those with a shorter wavelength. These three phenomena are connected through the dependence of wave energy and phase velocity on depth and wave height. Wave energy is dissipated as a result of boundary shear stresses at the bottom and at the water-air interface. A porous sand bottom will allow flow to occur in and out of the bottom. This can result in additional energy dissipation if the water is shallow.

In the development of wave theories, irrotational flow is assumed. This is a valid assumption since viscous forces are only present in the thin boundary layer found

at the sea surface and bottom, despite water being a viscous fluid. The governing equations and the necessary boundary conditions required in a water wave model are given in the next section.

2.2.1 Governing Equations

Classical linear water wave theory involves the following assumptions [2]

1. compressibility and viscosity in the fluid are neglected as well as surface tension at the free surface;

2. the fluid motion is assumed to be irrotational and can be described by a velocity potential $\phi(x, y, z, t)$;

3. nonlinear terms in the equations of motion and boundary conditions are neglected.

The equations resulting from the above assumptions are,

$$\frac{\partial u}{\partial x} + \frac{\partial v}{\partial y} + \frac{\partial w}{\partial z} = 0 \tag{2.9}$$

$$\nabla \times \mathbf{U} = 0 \tag{2.10}$$

$$\mathbf{U} = \nabla\phi \tag{2.11}$$

$$\textit{then} \quad \nabla^2\phi = 0 \tag{2.12}$$

$$\textit{where} \quad \mathbf{U} = (u(x, y, z, t), v(x, y, z, t), w(x, y, z, t)). \tag{2.13}$$

Since there is no flow normal to the bottom, the bottom boundary condition is

$$w = \frac{\partial\phi}{\partial z} = 0 \qquad \textit{at} \;\; z = -d. \tag{2.14}$$

Two boundary conditions can exist at the free surface. A kinematic boundary condition and a dynamic boundary condition. The kinematic boundary condition relates the vertical component of water particle velocity at the surface to the surface position,

$$w = \frac{\partial \eta}{\partial t} + u\frac{\partial \eta}{\partial x} + v\frac{\partial \eta}{\partial y} \qquad at\ z = \eta, \tag{2.15}$$

where η is the height of the surface above the still water level, u and v are the current velocity in the x and y -direction respectively and t is time. Nonlinear terms have been neglected according to linear water wave theory. Free surfaces cannot support variations in pressure across the air-water interface [8] therefore in order to maintain a uniform pressure along the interface a dynamic boundary condition has to be defined. The dynamic surface boundary condition is based on Bernoulli's equation for unsteady flow,

$$\frac{\partial \phi}{\partial t} + \frac{1}{2}(u^2 + v^2 + w^2) + \frac{p_\eta}{\rho} + gz = C(t), \tag{2.16}$$

where p_η is the pressure at the free surface, ρ is the water density and ϕ is the velocity potential. The current velocity components are represented by u, v and w, g the acceleration due to gravity and t is time. The pressure at the free surface is constant and usually taken as gauge pressure, $p_\eta = 0$. C(t) is the Bernoulli term. It is constant for steady flow. Once again the nonlinear terms have been left out.

When the depth varies with x, the Laplace equation cannot be reduced to a two dimensional equation. The mild slope equation was developed by Berkhoff (1972) to handle slowly varying bottom topography. The mild slope equation is a two dimensional elliptical partial differential equation that describes the complete transformation of small amplitude waves including refraction and diffraction. The Laplace

equation is vertically integrated to give the following equation,

$$\frac{\partial}{\partial x}(CC_g\frac{\partial \phi}{\partial x}) + \frac{\partial}{\partial y}(CC_g\frac{\partial \phi}{\partial y}) + \sigma^2\frac{C_g}{C}\phi = 0 \tag{2.17}$$

where C is the wave velocity, C_g is the wave group velocity and σ is the angular frequency. The wave group velocity is defined as the overall velocity of a group of ocean waves with different frequencies and wave velocities whereas, the wave velocity is the velocity of a single wave. The wave angular frequency , σ is defined as

$$\sigma^2 = gk\tanh kd, \tag{2.18}$$

where k is the wave number, d is the water depth and g the acceleration due to gravity.

Chapter 3

Sensitivity Analysis

For the case of open boundaries, the behavior of the model as less boundary data was available was investigated. The boundary data was obtained by running the model over a closed boundary basin. Simulations were then run with varying amounts of boundary data. At grid points where no boundary data was available a linear interpolation was carried out. Since small scale disturbance such as eddies are not modeled by the ocean circulation model the linear interpolation technique is sufficient. For the case of modeling the bottom topography a slightly more complex methodology was used. It involved the Karhunen-Loeve expansion and Polynomial Chaos expansion to generate the variability in the bottom topography being analyzed.

3.1 Karhunen-Loeve Expansion

The Karhunen-Loeve expansion of a stochastic process $E(x, \theta)$ is based on the spectral expansion of its covariance function $R_{EE}(x, y)$ [10] ,where x and y are spatial

coordinates and θ represents the random nature of the corresponding quantity. The expansion is defined as,

$$E(x,\theta) = \bar{E}(x) + \sum_{i=1}^{\infty} \sqrt{\lambda_i}\xi_i(\theta)\phi_i(x), \tag{3.1}$$

where $\bar{E}(x)$ is the mean of the stochastic process and $\xi_i(\theta)$ is an orthogonal set of random variables. The eigenfunctions and eigenvalues of the covariance kernel are represented by $\phi_i(x)$ and λ_i respectfully. The eigenfunctions are mutually orthogonal and form a complete set spanning the function space to which $E(x,\theta)$ belongs [10]. They can evaluated as the solution to the following integral equation

$$\int_{\mathcal{D}} R_{EE}(x,y)\phi_i(y)dy = \lambda_i\phi_i(x), \tag{3.2}$$

where $\mathcal{D}$ is the domain over which $E(x,\theta)$ is defined. The appeal of this spectral representation is that now the spatial random fluctuations have been decomposed into a set of deterministic functions in the spatial variables multiplying random coefficients that are independent of these variables. When a process is closer to white noise more terms are needed in its expansion but a random variable can be represented by a single term. The advantage of using the Karhunen-Loeve expansion is that, with only a few terms from the expansion one can capture most of the uncertainty in the process, since it can be assumed that material properties vary smoothly.

3.2 Polynomial Chaos Expansion

Polynomial Chaoses are polynomials in Gaussian random variables that describe the functional dependence of the nodal concentrations $c(\theta)$, for example wave height, to

the orthogonal set of random variables $\xi_i(\theta)$ that represents the material stochasticity [10]. This is expressed as

$$c(\theta) = a_0\Gamma_0 + \sum_{i_1=1}^{\infty} a_{i_1}\Gamma_1(\xi_{i_1}(\theta)) + \sum_{i_1=1}^{\infty}\sum_{i_2=1}^{i_1} a_{i_1 i_2}\Gamma_2(\xi_{i_1}(\theta), \xi_{i_2}(\theta)) + \cdots \tag{3.3}$$

where $\Gamma_n(\xi_{i_1}, \ldots, \xi_{i_n})$ is the Polynomial Chaos of order n in the Gaussian variables $(\xi_{i_1}, \ldots, \xi_{i_n})$. The pth order Polynomial Chaos can be expressed as,

$$\Gamma_p(\xi_{i_1}(\theta), \ldots, \xi_{i_n}(\theta)) = \begin{cases} \sum_{r=n}^{0}(-1)^r \sum_{\pi(i_1,\ldots,i_n)} \prod_{k=1}^{r} \xi_{i_k}(\theta) \prod_{l=r+1}^{n} \xi_{i_l}(\theta) & \text{n even} \\ \sum_{r=n}^{0}(-1)^{r-1} \sum_{\pi(i_1,\ldots,i_n)} \prod_{k=1}^{r} \xi_{i_k}(\theta) \prod_{l=r+1}^{n} \xi_{i_l}(\theta) & \text{n odd} \end{cases} \tag{3.4}$$

where $\pi(\cdot)$ denotes a permutation of its arguments and the sum is over all such permutations such that the set $(\xi_{i_1}, \ldots, \xi_{i_r})$ is modified by the permutation. The Polynomial Chaos expansion, when truncated after the pth term can be rewritten as,

$$c(\theta) = \sum_{j=0}^{p} c_j \Psi_j(\theta) \tag{3.5}$$

where c_j are deterministic coefficients and $\{\Psi_j(\theta)\}$ is a basis in the space of random variables. This basis is the set of generalized multidimensional Hermite polynomials. Due to the orthogonality of the Polynomial Chaoses the deterministic coefficient can be readily obtained by multiplying both sides of equation 3.5 by Ψ_i and averaging. Hence, the deterministic coefficients are determined using the following equation

$$c_j = \frac{< c\Psi_j >}{< \Psi_j^2 >} \tag{3.6}$$

where $< \cdot >$ represents the mean. The denominator of the equation has been tabulated [12].

Chapter 4

General Circulation Model

4.1 Introduction

This section refers to a numerical simulation model for solving the general circulation equations with specified boundary conditions. The model describes the large scale circulation of a closed basin. At the present it is run over a square basin measuring 2000 km by 2000 km by 2 km. The model can run up to a resolution of 240 by 240 by 24 grids and is run at a latitude of 45 deg. Hence the circulation pattern described by the model closely resembles the pattern seen in the North Atlantic. The open boundaries were implemented by splitting the basin in half such that one has outflow on the x boundary. The shallow water equations are solved in the model.

4.2 Shallow Water Equations

The model uses the shallow water equations to describe the circulation. The shallow water equations are a system of hyperbolic equations describing two classes of motion with different time scales. The "slow" Rossby-type (low frequency) motions and "fast" inertia-gravity (high frequency) motions. The former type of motions are considered to be significant, as they contribute the most to the energy of the system. Several methods have been developed to filter out the fast waves. In initialization, the underlying equations are kept but the initial pressure and velocity fields are adjusted so as to control the high frequency motions in a model. One initialization method that is of interest is the bounded derivative method developed by Kreiss (1979). The bounded derivative method can be applied to both global and limited-area models. Other initializations schemes such as the nonlinear normal mode initialization procedure can only be applied to a limited area under specific boundary conditions. Alternatively the equations can be transformed to only allow low frequency motions.

Browning [4] showed that only the large-scale boundary data needs to be correct in order to prevent the boundary error from propagating into the interior at the speed of the fast waves. The process of specifying data along the boundary of the regional model can be viewed as interpolating coarse data onto a fine grid. Given the sensitivity of the limited-area model to certain scales of boundary information, it is expected that different interpolation schemes may result in different modes of error propagation. Ultimately, it may be desirable especially given the sparsity of information on the coarse grid, to develop good stochastic interpolation schemes. In

the present study, however, and as a first step in that direction the significance of a variety of deterministic interpolation schemes is investigated.

The systems of equations used to describe shallow water behavior are usually derived from the Eulerian equations

$$\frac{ds}{dt} - \tilde{s}w = F_s \tag{4.1}$$

$$\frac{du}{dt} + \rho_0^{-1} p_x - f_0 v = F_u \tag{4.2}$$

$$\frac{dv}{dt} + \rho_0^{-1} p_y + f_0 u = F_v \tag{4.3}$$

$$\frac{dw}{dt} + \rho_0^{-1}(p_z + gs) = F_w \tag{4.4}$$

$$\frac{dp}{dt} + c^2 \rho_0 (u_x + v_y + w_z) = F_p \tag{4.5}$$

$$where \quad \frac{d}{dt} = \frac{\partial}{\partial t} + u\frac{\partial}{\partial x} + v\frac{\partial}{\partial y} + w\frac{\partial}{\partial z} \tag{4.6}$$

where ρ_0 is the mean density, p the pressure, u, v, w are the velocity components, f_0 is the Coriolis parameter. F is the forcing function, $\tilde{s}$ is the stratification parameter, s is the potential density and c is the speed of sound. The Coriolis parameter is given by

$$f = 2\Omega \sin\theta_0 + \frac{y}{r}\cos\theta_0$$

where $\Omega = 7.25 \times 10^{-5} s^{-1}$ is the earth's angular speed, r is the earth's radius and θ_0 is the latitude of the coordinate origin. For our case $\theta_0 = \frac{\pi}{4}$ and the Coriolis parameter is assumed to be constant. The potential density is a function of salinity and potential temperature. The potential temperature is defined as the temperature a parcel of water at depth would attain if it were adiabatically advected to the surface.

The potential density is expressed as

$$\begin{aligned} s &= 999.84 + 6.79 \times 10^{-2}\theta - 9.09 \times 10^{-3}\theta^2 \\ &+ 1.00 \times 10^{-4}\theta^3 - 1.12 \times 10^{-6}\theta^4 + 6.53 \times 10^{-9}\theta^5 \\ &+ (0.824493 - 4.0899 \times 10^{-3}\theta + 7.7438 \times 10^{-5}\theta^2 - 8.2467 \times 10^{-7}\theta^3 \\ &+ 5.3875 \times 10^{-9}\theta^4)S + (-5.72466 \times 10^{-3} + 1.0227 \times 10^{-4}\theta \\ &- 1.6546 \times 10^{-6}\theta^2)S^{1.5} + 4.8314 \times 10^{-4}S^2. \end{aligned} \tag{4.7}$$

In the above equation θ is the potential temperature in deg C and S is the salinity in practical salinity units. By making different assumptions, variations of the Eulerian system can be obtained. When hydrostatic and incompressible assumptions are made, the primitive system of equations is obtained. When the gravity and sound waves are slowed down one obtains the approximate system.

The most widely used systems to describe the shallow water equations are

1. Eulerian equations

2. Primitive equations - derived from the Eulerian equations by applying the hydrostatic and incompressible assumptions. A drawback of this system is that the open boundary problem is always ill posed.

3. Reduced system - derived from the approximate system in which the gravity and sound waves have been slowed down. Hence this set of equations only allow the low frequency motions to occur

The reduced system is the system of equations used in the NOAA code. The scaled

reduced system is

$$\frac{ds}{dt} - \tilde{s}w = 0 \tag{4.8}$$

$$\frac{du}{dt} + \epsilon^{-1}(p_x - fv) = F_u(y,z) \tag{4.9}$$

$$\frac{dv}{dt} + \epsilon^{-1}(p_y + fu) = 0 \tag{4.10}$$

$$\frac{dw}{dt} + \epsilon^{-2}(p_z + gs) = 0 \tag{4.11}$$

$$u_x + v_y + \epsilon w_z = 0, \tag{4.12}$$

where ϵ is the scaling parameter equal to the Rossby number and $\tilde{s} = 10^{-2}$.

In order to solve the shallow water equations, they first need to be scaled due to the different scales of motion they describe. The independent variables x, y, z and time are renormalized using the representative length and time scales. The dependent variables are scaled by their representative magnitudes. The shallow water equations are solved by applying the total time derivative to the continuity equation. An elliptic equation in terms of the pressure, p is obtained from this and the substitution of the equations of motion. The right hand side of the elliptical equation is a function of s, u, v, w and their first derivatives with respect to x, y and z.

$$p_{xx} + p_{yy} + p_{zz} = R(u,v,w,s), \tag{4.13}$$

where

$$R(u,v,w,s) = f(v_x - u_y) + 2(u_x v_y + u_x w_z + v_y w_z - u_y v_x - u_z w_x - v_z w_y) - \frac{\alpha g s_z}{\rho} - u\frac{df}{dy}. \tag{4.14}$$

The forcing function does not appear in the elliptical equation as it is a function in y and z only. The elliptical equation is solved using an elliptical solver from FISHPAK.

The velocity components and potential density are determined numerically using a leapfrog scheme,

$$\frac{k_i^{n+1} - k_i^{n-1}}{2\Delta t} = \frac{k_{i+1}^n - k_{i-1}^n}{2\Delta h} \tag{4.15}$$

where t is time, k is the property being solved for and Δh the increment of the property.

4.3 Boundary Conditions

The global model is an initial boundary value problem. It is run with solid boundaries on all four sides. At the boundaries the velocity normal to the boundary is set to zero.

$$u = 0 \text{ @ } x = \textit{west boundary},\ x = \textit{east boundary}$$

$$v = 0 \text{ @ } y = \textit{south boundary},\ y = \textit{north boundary}$$

At the sea surface and sea bed the boundary conditions satisfy the condition such that no water passes through the surface and sea bed respectively. The applied stress is zero at the sea bed. Neumann boundary conditions are specified for the global model

$$\frac{dp}{dx} = fv + F_u \tag{4.16}$$

$$\frac{dp}{dy} = -fu \tag{4.17}$$

$$\frac{dp}{dz} = \frac{-\alpha g s}{\rho}. \tag{4.18}$$

For the limited-area case, Dirichlet boundary conditions are specified on the open boundary. These conditions are obtained from post-processing the global model pre-

dictions.

4.4 Bounded Derivative Method

The bounded derivative method is an initialization process used to control high frequency motions. It is based on the observation that the solution, which varies slowly with respect to time, of a hyperbolic system with multiple time scales must have a number of time derivatives on the order of the slow time scale.

The bounded derivative method can be applied to both global and limited-area models. The principle steps used to determine the adjusted initial conditions are to,

1. define the characteristic space and time scales of the motion of interest,
2. perform a scale analysis of the time dependent system under consideration in order to identify terms that can contribute to large time derivatives,
3. constrain those terms to ensure that the time derivatives are of the low time scale, taking into account the boundary conditions.

4.5 Incorporating Topography

For simplicity, most ocean models are developed without bottom topography. In order to incorporate topography into the approximate systems the generalized vertical coordinate suggested by Kasahara [11] is used. It has the advantage of keeping the domain of integration regular and of allowing considerable freedom in the placement

of the vertical mesh points. The independent variables are transformed

$$t = t' \tag{4.19}$$

$$x = x' \tag{4.20}$$

$$y = y' \tag{4.21}$$

$$z = z(x', y', z'). \tag{4.22}$$

The velocity components are obtained by applying the total derivative operator to (4.20)-(4.22) to obtain

$$u' = u \tag{4.23}$$

$$v' = v \tag{4.24}$$

$$w' = z'_z(w - z_{x'}u' - z_{y'}v'). \tag{4.25}$$

In the transformed coordinate the approximate system is

$$\frac{ds}{dt'} - \tilde{s}w = 0 \tag{4.26}$$

$$\frac{du}{dt'} + \rho_0^{-1}(p_{x'} - z_{x'}z'_z p_{z'}) - fv = 0 \tag{4.27}$$

$$\frac{dv}{dt'} + \rho_0^{-1}(p_{y'} - z_{y'}z'_z p_{z'}) + fu = 0 \tag{4.28}$$

$$\frac{dw}{dt'} + \alpha[\rho_0^{-1}z'_z p_{z'} + g(\gamma p_0)^{-1}p + gs] = 0 \tag{4.29}$$

$$\frac{dp}{dt'} + \gamma p_0[u_{x'} - z_{x'}z'_z u_{z'} + v_{x'} - z_{y'}z'_z v_z + z'_z w_{z'}] - g\rho_0 w = 0, \tag{4.30}$$

where

$$\frac{d}{dt'} = \frac{\partial}{\partial t'} + u\frac{\partial}{\partial x'} + v\frac{\partial}{\partial y'} + w\frac{\partial}{\partial z'}, \quad s \equiv \frac{\rho p^{-1/\gamma} - s_0}{s_0} \tag{4.31}$$

The system is valid for all time scales because the unapproximated forms of equations (4.27) and (4.28) are used. In the large scale case a hydrostatic approximation is used

to replace $z'_z p_{z'}$. This approximation is invalid for the small scale case.

To develop a three dimensional flow, the untransformed Eulerian equations are linearized about an isothermal ocean at rest. This results in the linear constant coefficient system

$$\frac{ds}{dt} - \tilde{s}w = 0 \tag{4.32}$$

$$\frac{du}{dt} + \rho_0^{-1} p_x - f_0 v = 0 \tag{4.33}$$

$$\frac{dv}{dt} + \rho_0^{-1} p_y + f_0 u = 0 \tag{4.34}$$

$$\frac{dw}{dt} + \rho_0^{-1} p_z + gs = 0 \tag{4.35}$$

$$\frac{dp}{dt} + \gamma p_0 (u_x + v_y + w_z) = 0 \tag{4.36}$$

The bounded derivative constraints obtained from requiring that the first order time derivatives be of order unity is that the flow is geostrophic, hydrostatic and totally nondivergent. Hence

$$u = -\psi_y \tag{4.37}$$

$$v = \psi_x \tag{4.38}$$

$$\phi = f_0 \psi \tag{4.39}$$

$$s = -(g\rho_0)^{-1} p_z, \tag{4.40}$$

where $\psi(x, y, z)$ is a given streamfunction. In the present analysis, the bottom topography in the circulation model is assumed constant and flat.

4.6 Sensitivity Analysis

A global model with a coarse grid resolution of 20 x 20 x 8 was first run to obtain the necessary boundary data. The limited-area model was a basin of 10 x 20 x 8, with the open boundary on the outflow side. Four limited-area cases were run. In the first case, all the boundary data from the global model was passed to the limited-area model. In the second case, only every other boundary data point was passed to the limited-area model. Linear interpolation was used to approximate the data at the missed points. In the third and fourth cases only five and three boundary data points were read in respectively. Once again data for the missed grid points was interpolated from the inputted boundary data.

4.7 Results

A full basin model of grid dimensions 20 x 20 x 8 was run. Using the contour plots of the horizontal velocity u as an indicator the implementation of the open boundaries seems reasonable. For the one and two open boundary cases the behavior agrees at the second time step. Figures 4.1 - 4.3 show contour plots of a full basin run, a half-basin run with the open boundary on the eastern boundary and a three-quarters basin run with open boundaries on the east and north boundary. From Figures 4.2 and 4.3 we observe an exact replication of the global circulation in a limited-area. A half-basin is used to analyses the behavior of the open boundary. When the model is left to run for longer periods we see an exponential increase in the error. The error plot for our four open boundary conditions is shown in Figure 4.4. The solid

line represents data taken at point (6,16) on a horizontal plane. The dashed line is data taken at point (6,11). As mentioned earlier, only the boundary data needs to be accurate in order to prevent error from destroying the solution. However we see that this is not entirely true. In the error plot where boundary data from all points were passed to the limited-area model, we observe error entering the solution at an increasing rate.

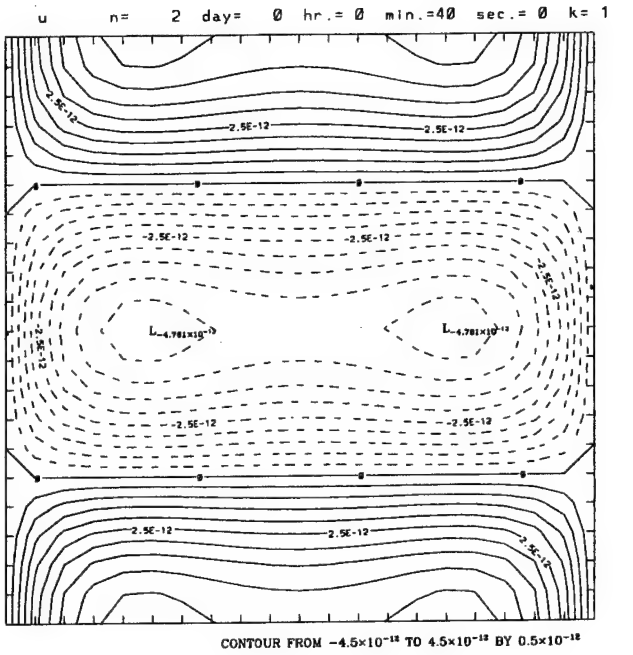

Figure 4.1: Contour plot of the horizontal velocity component, u over the entire basin at the first time step

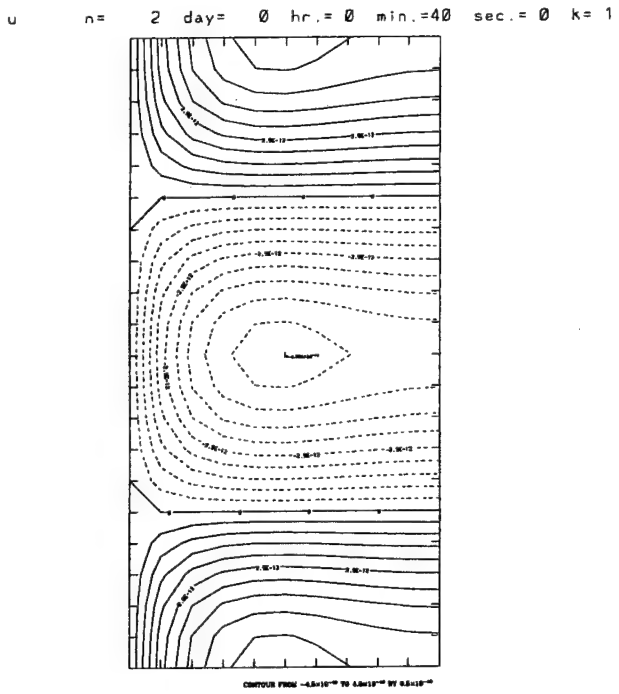

Figure 4.2: Contour plot of the horizontal velocity component, u over half the basin with one open boundary, at the first time step

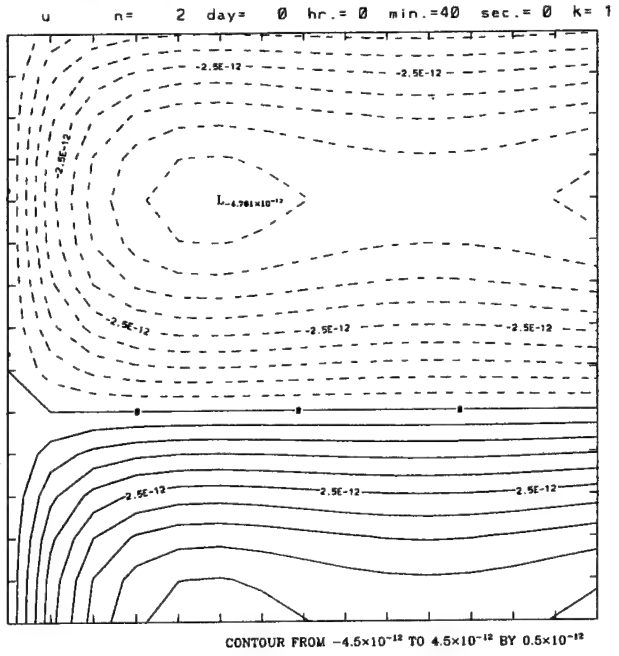

Figure 4.3: Contour plot of the horizontal velocity component, u over three-quarters of the basin with two open boundaries at the first time step

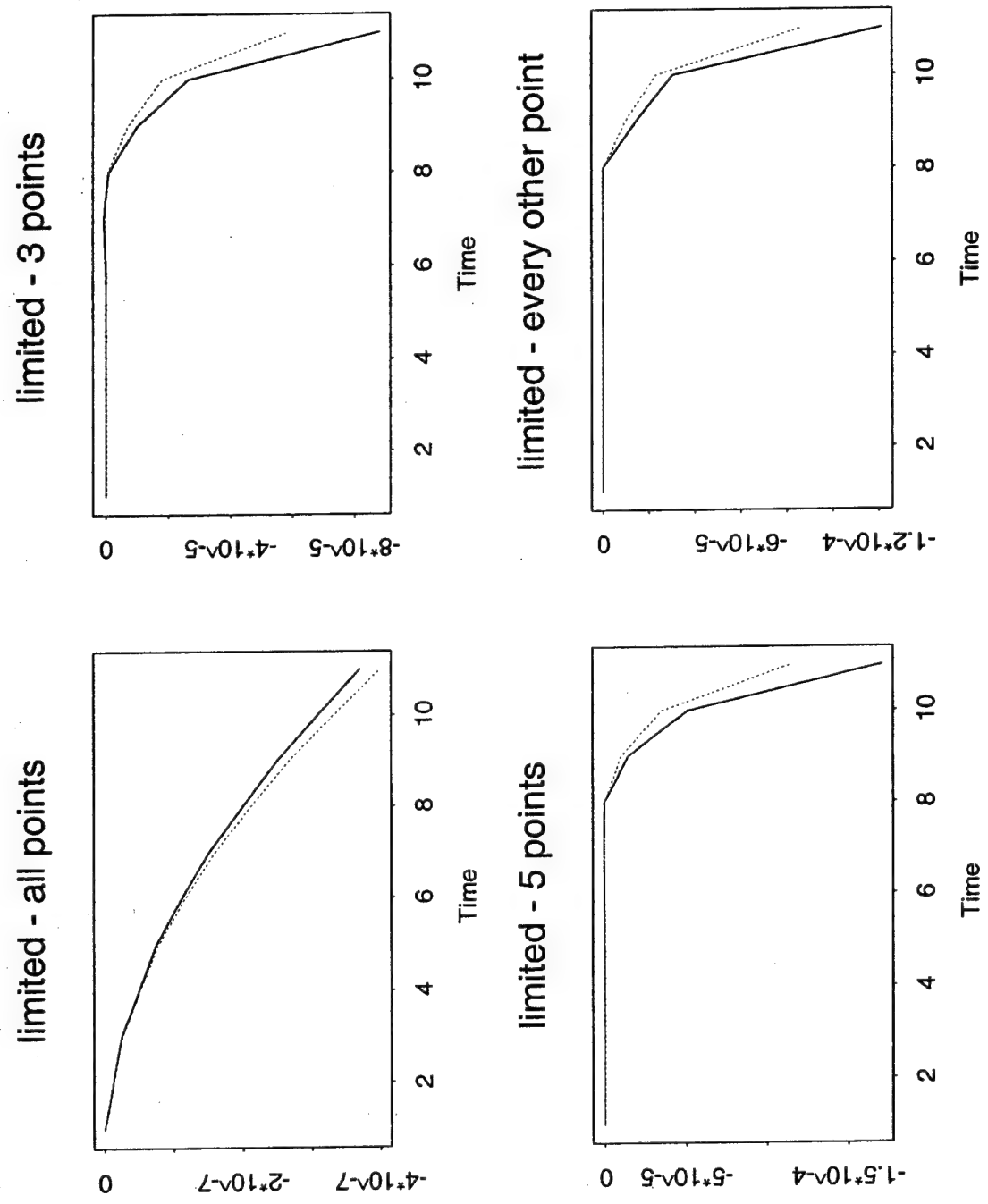

Figure 4.4: Propagation of error with time

Chapter 5

Water Wave Model

5.1 Ref/Dif 1

Ref/Dif 1 combines both the effects of refraction and diffraction explicitly, making it ideal for the modeling of ocean waves in regions of irregular bottom topography and in regions where diffraction is important [6]. In previous models in order to incorporate diffraction, refraction was suspended in the regions where diffraction was dominant. This method was inaccurate but it allowed for the inclusion of diffraction. Ray tracing techniques were used for the analysis of refraction of water waves. These techniques were inaccurate whenever diffraction effects were important, since they do not include diffraction. These techniques also predicted infinite wave heights at the point of intersecting wave rays as a result of complex bottom topography. Ref/Dif 1 includes the following effects [6]

1. Parabolic approximation:

(a) Minimax approximation

2. Wave nonlinearity:

   (a) Linear

   (b) Composite nonlinear

   (c) Stokes nonlinear

3. Wave breaking

4. Absorbing structures and shorelines:

   (a) Thin film model surrounded by a natural surf-zone

5. Energy dissipation:

   (a) Turbulent bottom friction damping

   (b) Porous bottom damping

   (c) Laminar boundary layer damping

6. Lateral boundary conditions:

   (a) Reflective condition

   (b) Open boundary condition

7. Input wave field:

   (a) Model specification of monochromatic or directional wave field.

   (b) Input of initial row of data from disk file.

8. Output wave field:

   (a) Standard output

   (b) Optional storage of last full calculated row of complex amplitudes.

5.2 Mild slope equation

Very few solutions exist for the three dimensional problem of water waves propagating over irregular bathymetry. This problem involves complicated nonlinear boundary conditions. In order to simplify the problem it was reduced to a problem of two horizontal dimensions. This was achieved by vertically integrating the model. Furthermore, the important properties of linear progressive waves could be predicted. The linear mild slope equation is

$$\frac{\partial}{\partial x}(CC_g\frac{\partial \phi}{\partial x}) + \frac{\partial}{\partial y}(CC_g\frac{\partial \phi}{\partial y}) + \sigma^2\frac{C_g}{C}\phi = 0 \tag{5.1}$$

where C is the wave velocity, C_g is the group velocity, ϕ is the velocity potential and σ is the angular frequency.

The model equation assumes that the variations in the bottom occur over distances which are long in comparison to a wave length. A comparison carried out by Booij (1983) found that the mild slope model was accurate for bottom slopes up to 1:3.

The model equation used in Ref/Dif 1 is a version of the mild slope equation that includes the influence of current. The equation also includes the minimax approximation, which is the minimization of the maximum error for a rixed number of terms

and is expressed as,

$$
\begin{aligned}
(C_g+U)A_x \;-\; & 2\Delta_1 V A_y + i(\bar{k}-a_0k)(C_g+U)A + \left\{\frac{\sigma}{2}\left(\frac{C_g+U}{\sigma}\right)_x - \Delta_1\sigma\left(\frac{V}{\sigma}\right)_y\right\}A \\
+\; & i\Delta'\left[(p-V^2)\left(\frac{A}{\sigma}\right)_y\right]_y - i\Delta_1\left\{\left[UV\left(\frac{A}{\sigma}\right)_y\right]_x + \left[UV\left(\frac{A}{\sigma}\right)_x\right]_y\right\} \\
+\; & \frac{i\sigma k^2}{2}D|A|^2A + \frac{w}{2}A + \frac{-b_1}{k}\left\{\left[(p-V^2)\left(\frac{A}{\sigma}\right)_y\right]_{yx} + 2i\left(\sigma V\left(\frac{A}{\sigma}\right)_y\right)_x\right\} \\
+\; & b_1\beta\left\{2i\omega U\left(\frac{A}{\sigma}\right)_x + 2i\sigma V\left(\frac{A}{\sigma}\right)_y - 2UV\left(\frac{A}{\sigma}\right)_{xy} + \left[(p-V^2)\left(\frac{A}{\sigma}\right)_y\right]_y\right\} \\
-\; & \frac{i}{k}b_1\{(\omega V)_y + 3(\omega U)_x\}\left(\frac{A}{\sigma}\right)_x - \Delta_2\left\{\omega U\left(\frac{A}{\sigma}\right)_x + \frac{1}{2}\omega U\left(\frac{A}{\sigma}\right)\right\} \\
+\; & ik\omega U(a_0-1)\left(\frac{A}{\sigma}\right) = 0, \qquad (5.2)
\end{aligned}
$$

where

$$\beta = \frac{k_x}{k^2} + \frac{(k(p-U^2))_x}{2k^2(p-U^2)}$$

$$\Delta_1 = a_1 - b_1$$

$$\Delta_2 = 1 + 2a_1 - 2b_1$$

$$\Delta' = a_1 - b_1\frac{\bar{k}}{k}$$

and $p = CC_g$, U is the mean current velocity in the x direction, V is in the y direction, $\bar{k}$ is the average wave number along the y axis, ω is a dissipation factor that is discussed in the next section and A is a complex amplitude related to the water surface displacement by

$$\eta = Ae^{i(kx-\sigma t)} \qquad (5.3)$$

In the above equation η is the surface displacement. The term D is given by,

$$D = \frac{(\cosh 4kh + 8 - 2\tanh^2 kh)}{8\sinh^4 kh} \qquad (5.4)$$

The coefficients a_0, a_1 and b_1 depend on the aperture width [6] chosen to specify the minimax approximation. However, the model uses the Pade approximation based on the following coefficients

$$a_0 = 1 \tag{5.5}$$

$$a_1 = -0.75 \tag{5.6}$$

$$b_1 = -0.25. \tag{5.7}$$

Since the model follows a Stokes expansion it is only valid for Stokes waves. Consequently in order to have a valid model in shallow water a heuristic dispersion relationship developed by Hedges (1976) is used. The final model has a dispersion relationship that is a smooth patch between the Hedges form and Stokes relationship.

5.3 Energy dissipation

Ref/Dif 1 is able to treat energy losses due to bottom friction, surface films and wave breaking. The type of energy loss determines the form of the dissipation factor, ω. For turbulent bottom boundary friction the dissipation factor is

$$\omega = \frac{2\sigma k f |A|(1-i)}{3\pi \sinh 2kh \sinh kh} \tag{5.8}$$

The Darcy-Weisbach friction factor, f is set to 0.01. For porous bottom damping the dissipation factor is

$$\omega = \frac{gkC_p(1-i)}{\cosh^2 kh} \tag{5.9}$$

where C_p is the coefficient of permeability and is of the order 4.5×10^{-11} m^2 and g is the acceleration due to gravity. Laminar boundary layer damping occurs both at

the water surface and the bottom. It is a result of viscosity. Surface boundary layer damping occurs due to surface films. Surface film damping is

$$\omega = \frac{\sigma\sqrt{\nu/2\sigma}(1-i)}{\tanh kh} \tag{5.10}$$

where ν is the kinematic viscosity. The term under the square root sign is related to the thickness of the boundary layer [6]. At the bottom the boundary layer damping is

$$\omega = \frac{\sigma\sqrt{\nu/2\sigma}(1-i)}{\sinh kh} \tag{5.11}$$

The wave breaking algorithm is always active in the model. The dissipation due to wave breaking is given by

$$\omega = \frac{KC_g(1-(\gamma h/H)^2)}{h} \tag{5.12}$$

where K and γ are arbitrary constants determined to equal 0.017 and 0.4 respectively.

5.4 Bottom Topography

In order to run Ref/Dif 1 with a random bottom, the physics based assumptions used by the model were not altered. The depth data in the output data file, refdat.dat, was changed to reflect the variable bottom topography. The Karhunen-Loeve expansion was used to represent the randomness in the bottom topography. Ten Gaussian variables, ξ_i were used to represent the stochasticity in the bottom topography. The elevation of the bottom was consider to be a random property that could be expanded as follows,

$$\mathbf{k}(\mathbf{x},\theta) = \sum_{i=0}^{10} \xi_i(\theta)\mathbf{k_i}(\mathbf{x}) \tag{5.13}$$

where $\mathbf{k}$ is the elevation of the bottom, $\mathbf{k_i}$ represents a certain scale of fluctuation of bottom elevation and ξ_i represents the random contribution to the overall property. The 10 eigenmodes used to generate the bottom topography are shown in Figures 7-17. Various solution quantities were then represented in terms of their Polynomial Chaos decomposition as,

$$c(x,t,\theta) = \sum_{i=0}^{p} c_i(x,t)\Psi_i(\theta) \tag{5.14}$$

where $c_i(x,t)$ are deterministic quantities and $\{\Psi_i(\theta)\}$ is a basis in the space of random variables. As mentioned earlier in our discussion of the Polynomial Chaos expansion, the basis is taken to be the set of generalized multidimensional Hermite Polynomials in the quantities $\xi_i(\theta)$. Since the ξ_i values have a Gaussian distribution it is expected that the depth of the model will also follow a Gaussian distribution. The Polynomial chaos expansion was then used for the wave height, wave angle and bottom velocity data. We are interested in seeing the type of distribution these quantities will now have. Furthermore, since the mild slope equation is accurate for slopes not greater than 1:3, the behavior of the model as it experiences steeper slopes should be interpreted with care.

200 simulations of Ref/Dif 1 were performed. In order to determine the coefficients c_i, equation 5.14 was divided by Ψ_i and averaged

$$< c\Psi_i >= c_i < \Psi_i^2 > \tag{5.15}$$

The right hand side of the above equation can be expressed as,

$$< c\Psi_i >= \frac{1}{N}\sum_{r=1}^{N} c_r \Psi_j^{(r)} \tag{5.16}$$

where r denotes the simulation run. After employing the above equation, the coefficients c_i are determined using equation 3.6.

5.5 Results

Ref/Dif 1 was run to simulate the behavior of waves around an artificial island. 200 simulation runs were performed. The island is circular with a base radius of 400 ft. The mean water depth around the island is 30 ft. The wave conditions modeled were a wave height of 28 ft (see figure 2) and a wave period of 10 seconds. On input, the file containing the constant depth data was substituted for one that contained variable depth data. Only 20 of the Hermite Polynomials were used to generate the bottom topography. Ref/Dif 1 produces output files that give information about the wave height, the water depth with tide correction, wave angle, magnitude of the bottom velocity and an instantaneous snapshot of the water surface. Interest lies in how a randomly generated bottom topography will affect the results from Ref/Dif 1. Prior to running the 200 simulations, the model of the island was run with a flat bottom topography. The results from this run are shown in Figures 5.11 - 5.14. In Figures 5.12 and 5.13 the dashed lines are contours of the bottom topography and the solid lines are contours of wave height and the instantaneous water surface respectively. Due to the architecture of Ref/Dif 1, we assume that the bottom topography to the left of the island is the same as that to the right of the island. Since the behavior of the water waves will be symmetric only half the island is shown by Ref/Dif 1. The waves are incident on the island from the left side of Figures 5.12-5.14.

The results from the first simulation are shown in Figures 5.15 - 5.17. Figure 5.15 shows a realization of the bottom topography. A plot of what the water surface looks like is given by Figure 5.16. The water waves are incident on the island from the left

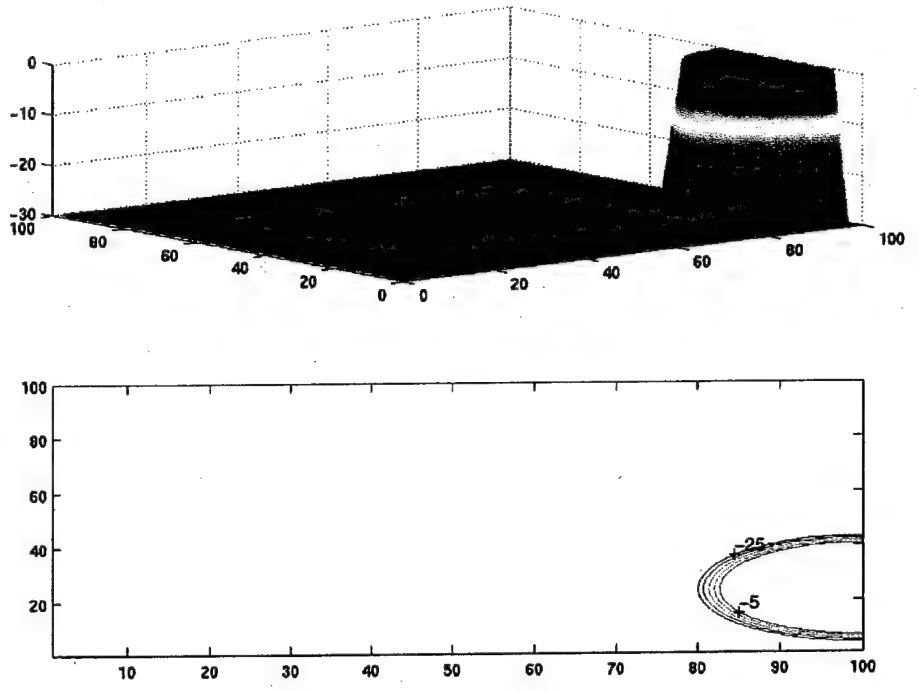

Figure 5.11: Bottom topography for flat bottomed model

hand side of Figure 5.18. The diffraction of the water fronts as they encounter the island is visible.

The probability density was evaluated for the wave height, water depth, wave angle and surface (see Figure 5.19). The probability density of the wave angle seems to follow a Gaussian distribution. The water depth shows a very skewed distribution as expected with its peak occurring around 31 ft. The density plot of the wave height is a multimodal distribution with three peaks. Its highest peak occurs at 12 ft.

The Polynomial Chaos expansion was truncated after the 21st term for each property. The first term in the expansion represented the mean of the property. The subsequent summation of the square of the remaining twenty terms yielded the variance of the property.

Figures 5.24 - 5.27 are plots of the variance for the properties.

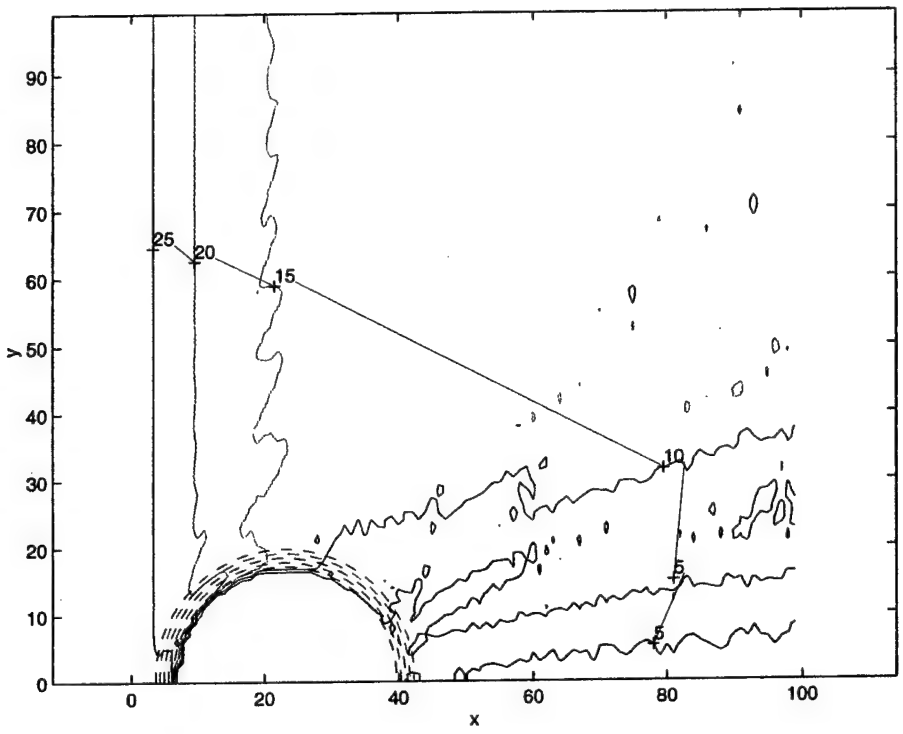

Figure 5.12: Plot of wave height for flat bottomed model

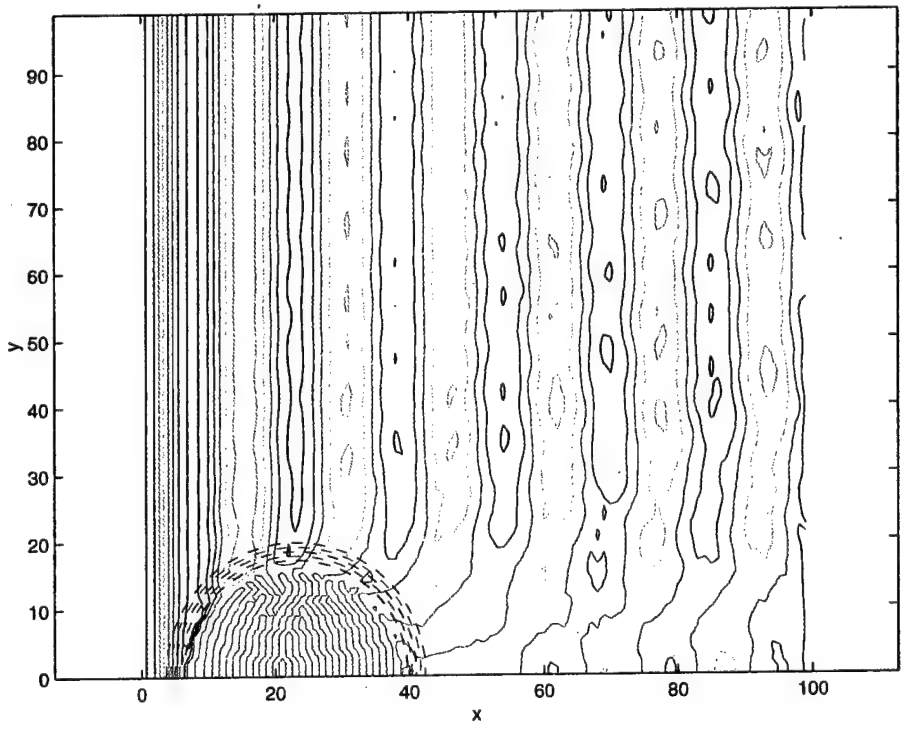

Figure 5.13: Surface plot of flat bottomed model

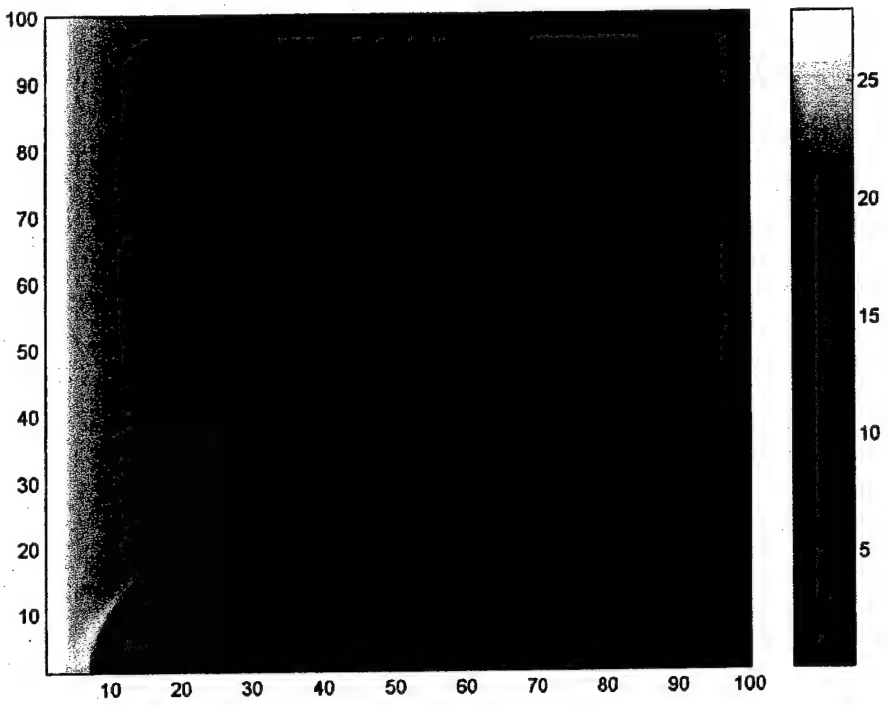

Figure 5.14: Rendering of water surface for the flat bottomed model

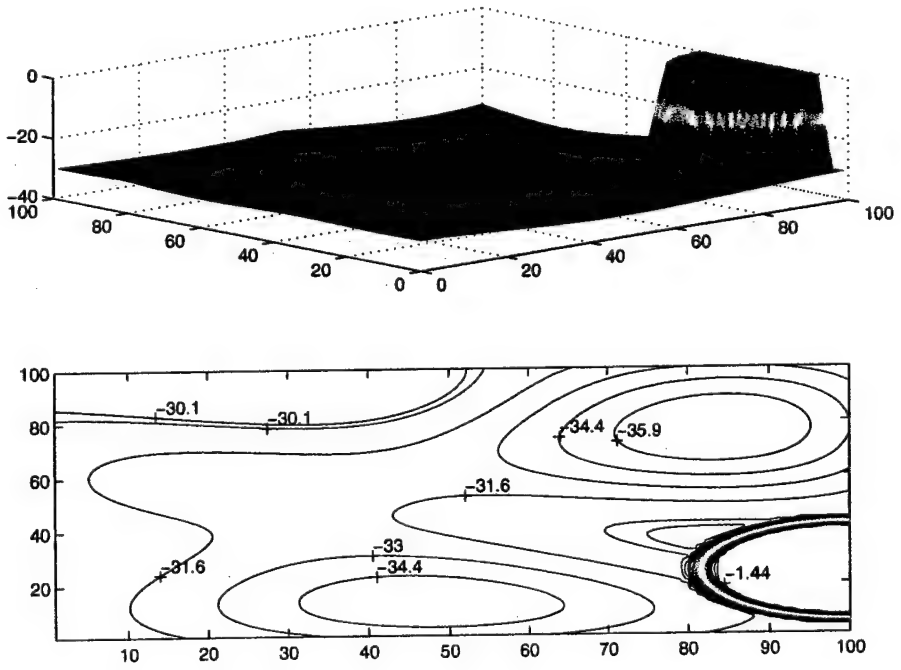

Figure 5.15: Bottom topography of first simulation

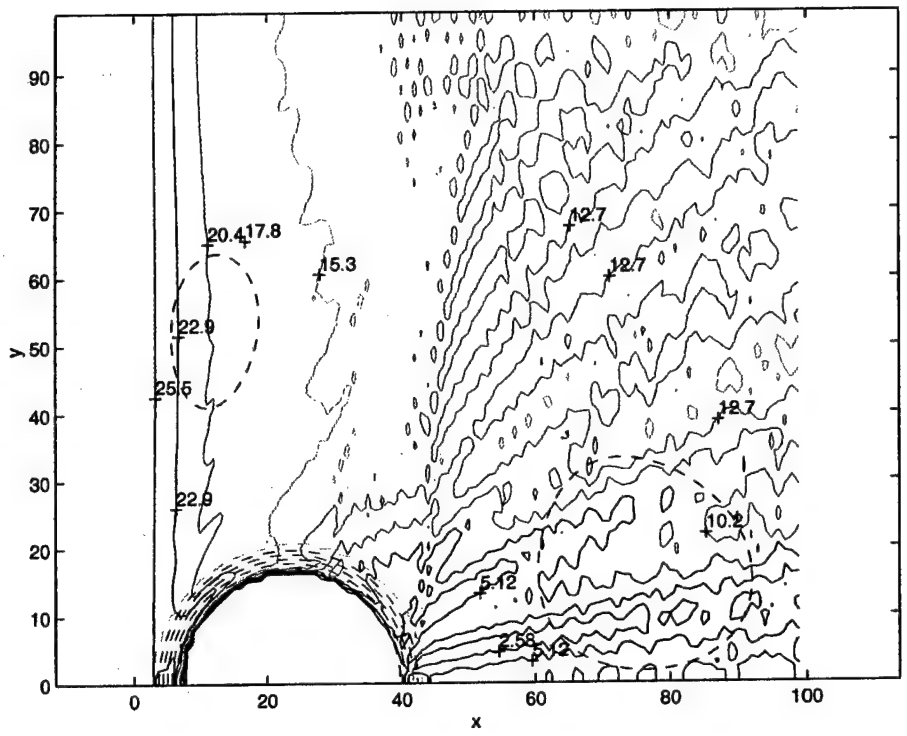

Figure 5.16: Plot of wave height from first simulation

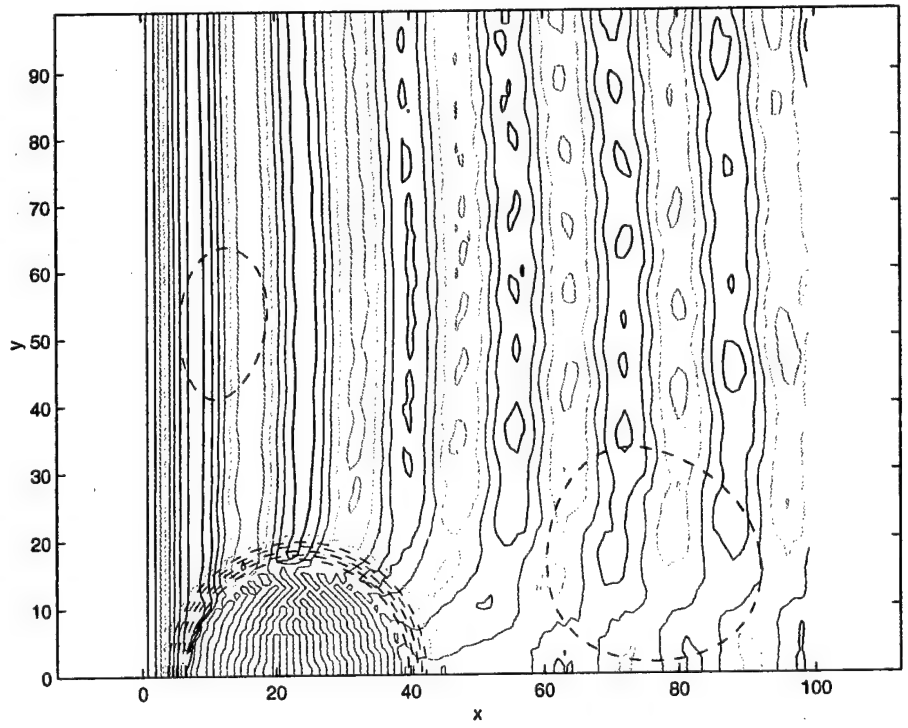

Figure 5.17: Surface plot of first simulation

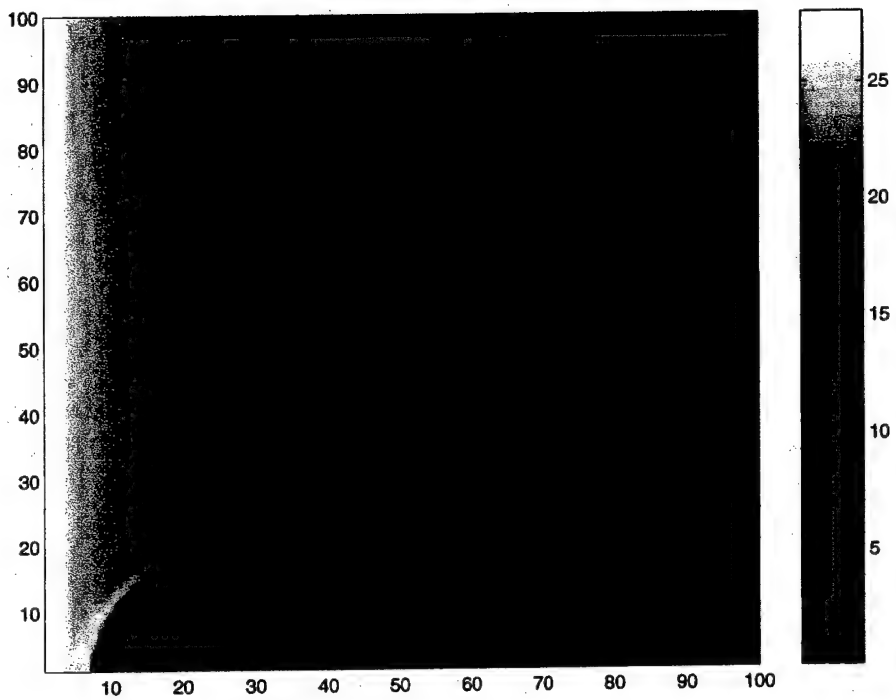

Figure 5.18: Rendering of water surface of the first simulation

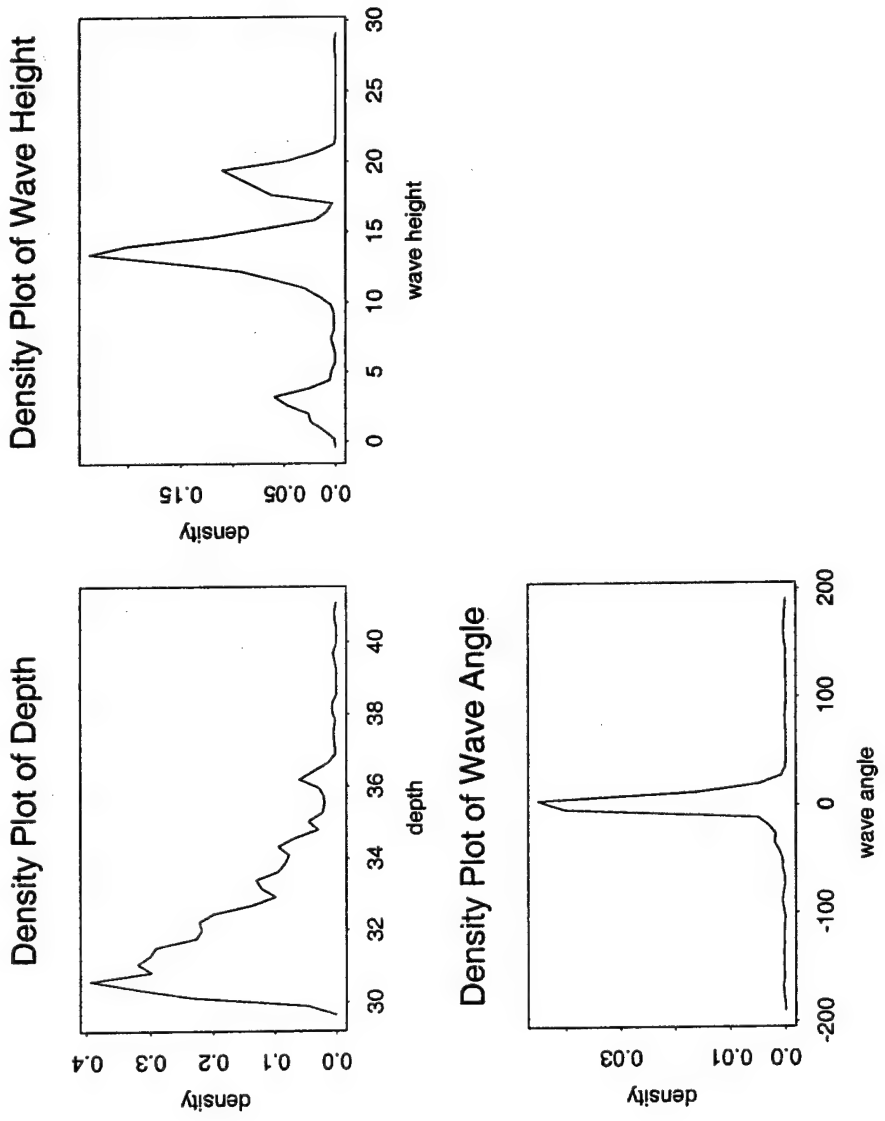

Figure 5.19: Probability density

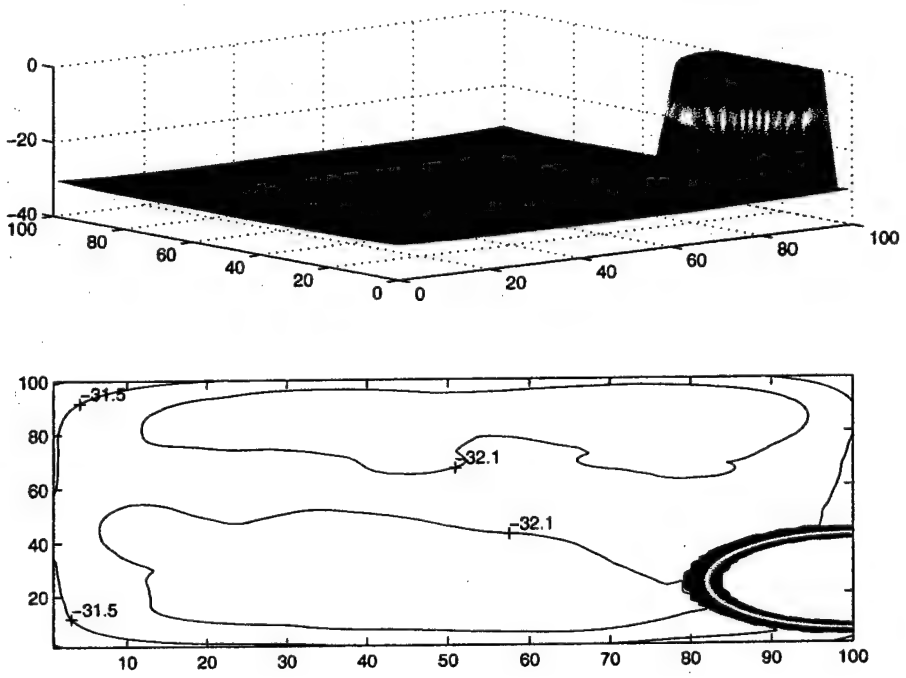

Figure 5.20: Mean topography

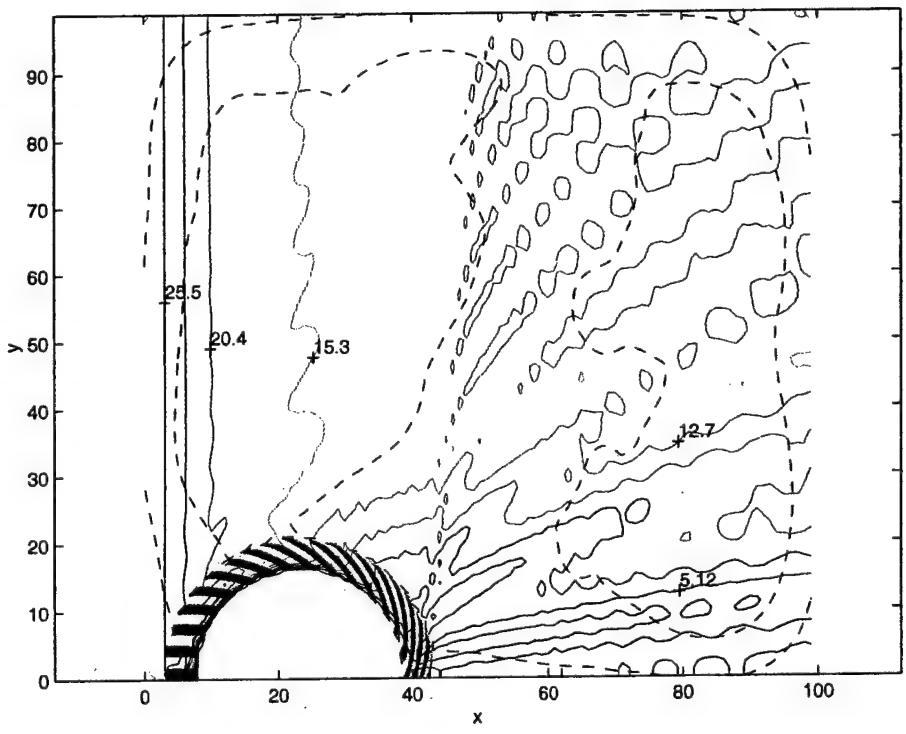

Figure 5.21: Mean wave Height

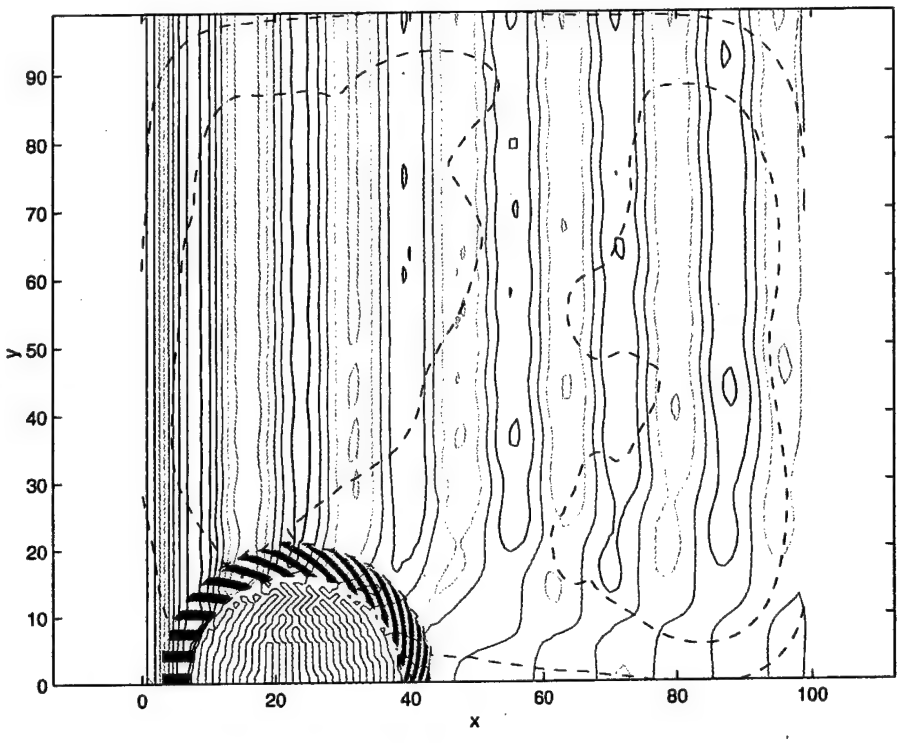

Figure 5.22: Mean surface

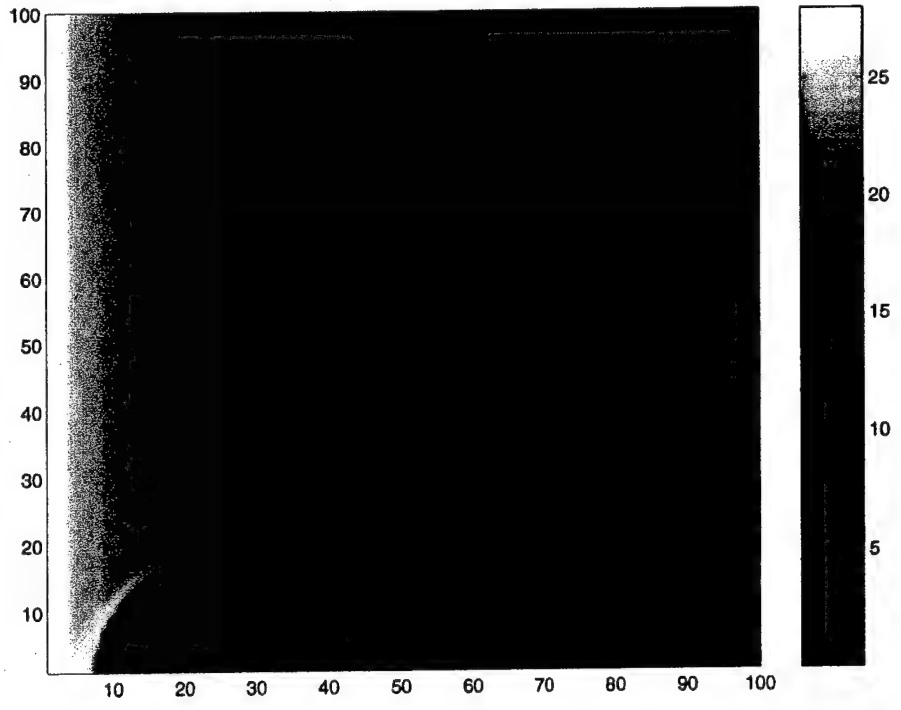

Figure 5.23: Mean surface

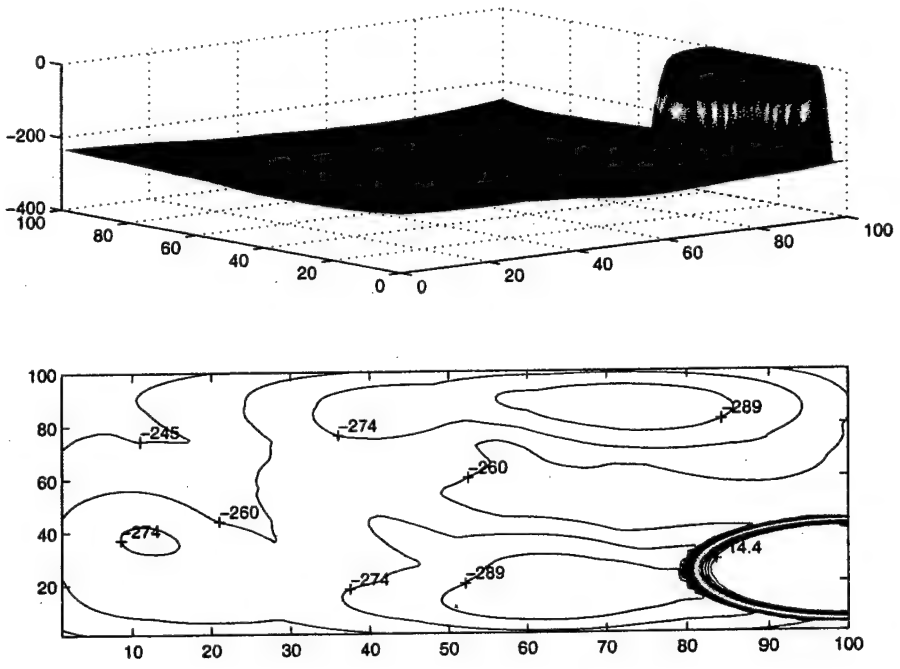

Figure 5.24: Negative variance of bottom topography

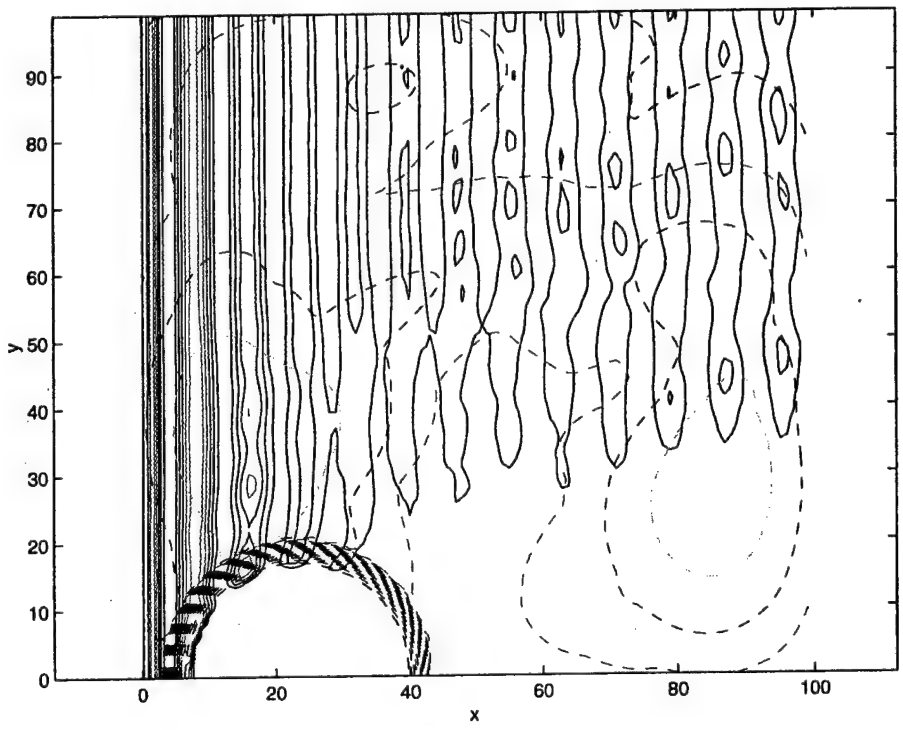

Figure 5.25: Variance of surface

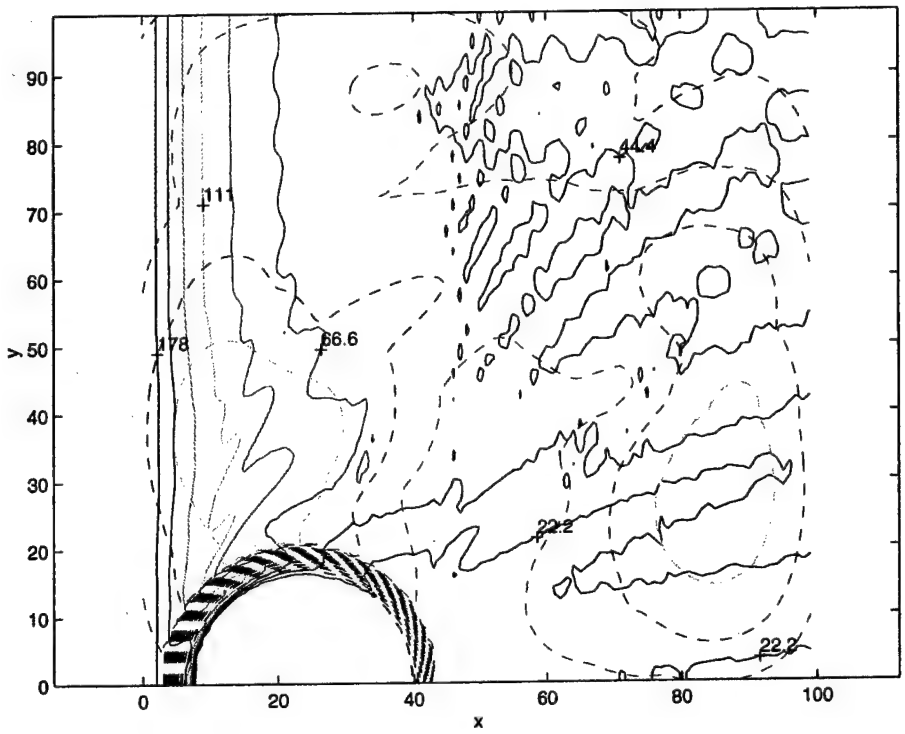

Figure 5.26: Variance of wave height

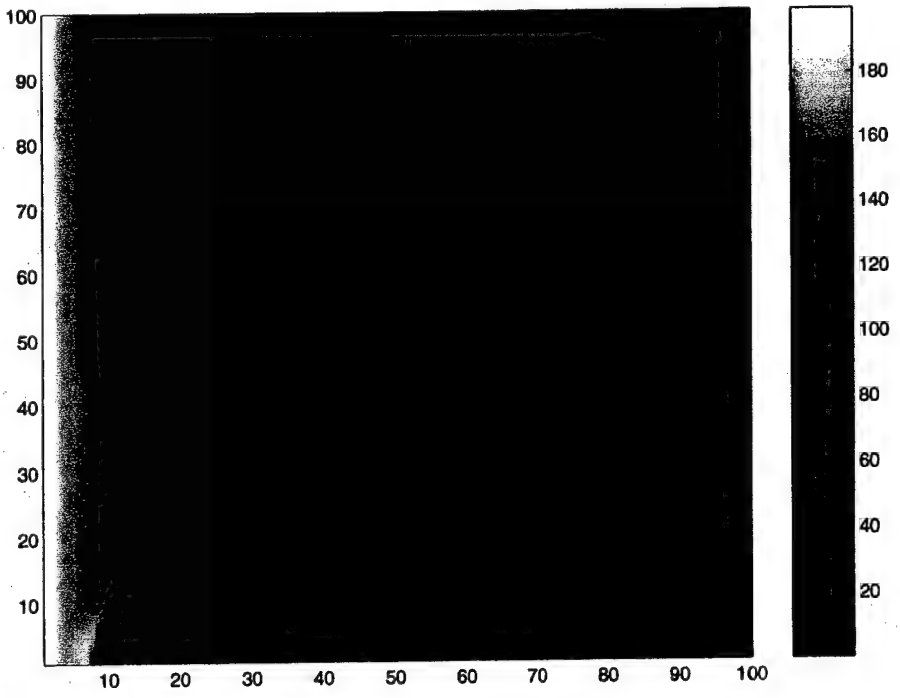

Figure 5.27: Variance of surface

Chapter 6

Conclusion

For the limited-area model, error was observed in the solution even when all the boundary data was passed to the limited-area model. This hints that on top of the need for accurate boundary data, the initial data might need to be initialized by the bounded derivative method, for example, to ensure that error does not propagate into the solution.

It has been shown that variability in the bottom topography does not affect the results obtained from Ref/Dif 1. The density plots of the wave height and water depth concur with the mean and variance plots of the wave height and bottom topography. Furthermore, a comparison of the mean solution to the deterministic solution shows that the random bottom topography had little effect on the Ref/Dif 1 results.

Bibliography

[1] Sorenson, R.M. (1993), *Basic Wave Mechanics: For Coastal and Ocean Engineers*, John Wiley & Sons, Inc.

[2] Hunt, J.N. (ed.) (1997), *Gravity Waves in Water if Finite Depth.* Advances in Fluid Mechanics

[3] Browning, G.L. and MacDonald, A.E. (1993), "Incorporating topography into the multiscale systems for the atmosphere and oceans," *Dynamics of Atmospheres and Oceans*, 18: 119-149,

[4] Browning, G. and Kreiss, H.-O. (1982), "Initialization of the shallow water equations with open boundaries by the bounded derivative method," *Tellus* 34: 334-351.

[5] Browning, G.L., Holland, W.R.and Kreiss, H.-O. (1992) " A comparison of differential systems and numerical methods for the computation of smooth oceanographic flows," *Dynamics Of Atmospheres and Oceans* 16: 499-526.

[6] Kirby, J.T. and Dalrymple, R.A, (1994), "Combined Refraction/Diffraction Model, Documentation and User's Manual," CACR Report No. 94-22.

[7] Kirby, J.T. and Dalrymple, R.A. (1983), "A parabolic equation for the combined refraction-diffraction of Stokes waves by mildly varying topography," *Journal of Fluid Mechanics*, 136: 453-466

[8] Dean, R.G. and Dalrymple, R.A. (1984), *Water Wave Mechanics for Engineers and Scientists*, Prentice-Hall, NJ.

[9] Mellor, G.L. (1996), *Introduction to Physical Oceanography*, Springer, NY

[10] Ghanem, R. (1998), "Probabilistic characterization of transport in heterogeneous media", *Computer Methods in Applied Mechanics and Engineering*, 158: 199-220.

[11] Kasahara, A. (1974), "Various vertical coordinate systems used for numerical weather prediction," *Monthly Weather Review*, 102: 509-522.

[12] Ghanem, R. and Spanos, P. (1991), *Stochastic Finite Elements: A Spectral Approach*, Springer Verlag

Vita

Dubar Kamara was born on March 28, 1979 in Sierra Leone. She attended Johns Hopkins University where she received her Bachelors in 2001. Currently she is a candidate for a Master of Science.